Hydrodynamic coupling drives bacterial flagellar synchrony

Tsubasa Ishihara[1], Nariya Uchida[2,*], and Shuichi Nakamura[1,*]

[1]Department of Applied Physics, Graduate School of Engineering, Tohoku University
[2]Department of Physics, Graduate School of Science, Tohoku University
[*]Corresponding authors: nariya.uchida.c1@tohoku.ac.jp, shuichi.nakamura.e8@tohoku.ac.jp

Synchronization is a fundamental phenomenon observed across a wide range of physical, chemical, and biological systems. Even under the low-Reynolds-number conditions that govern microbial motility, synchronization of rhythmic processes is considered essential for diverse activities ranging from single cells to populations, yet experimental evidence remains scarce. Here, we measured bacterial flagellar dynamics at the level of single motor units, revealing a synchronization phenomenon among nanoscale molecular machines. The observed intermittent in-phase synchronization was analyzed using a novel hydrodynamic model incorporating elastic deformation of the flagella, showing that stronger hydrodynamic coupling promotes more stable phase-locking. These findings suggest that synchronized rotation induced by weak and intermittently repeated fluid-mediated interactions could facilitate flagellar bundle formation and enhance swimming efficiency. This study bridges functional molecular nanomachines in living cells and nonlinear dynamics, providing a new physical perspective on synchronization in active biological systems.

Introduction

Synchronized motion of periodic locomotor organs, such as legs, wings, and flagella, underlies directional locomotion across biological systems. In animals, such coordination is typically achieved through the interplay of sensory information and neural circuits [1, 2], while vortex-mediated interactions also induce phase matching in bird flocks [3] and fish schools [4–7]. In contrast, microorganisms lack a nervous system, and their synchronization must arise from fundamental physical principles. Indeed, at microscopic scales—where viscous forces dominate and inertia is negligible—synchronization is known to emerge from purely hydrodynamic interactions. A classical example is the metachronal wave generated by coordinated beating of cilia on the surface of *Paramecium*, which drives forward swimming through a traveling wave of net flow [8]. In the green alga *Chlamydomonas*, two eukaryotic flagella beat synchronously in a breast-stroke-like pattern [9, 10]. Such synchronous beating of cilia and flagella has long been attributed to hydrodynamic coupling, a mechanism first proposed by Taylor in his seminal theoretical work [11]. Recent studies, however, suggest that synchronization may also involve non-hydrodynamic factors. For example, the metachronal coordination in *Paramecium* is influenced by cell surface elasticity [12], and body rocking contributes to flagellar synchronization in *Chlamydomonas* [13].

Bacterial flagella, by contrast, are fundamentally different from their eukaryotic counterparts. Each flagellum consists of a helical filament that functions as a screw-like propeller, rotated by a membrane-embedded flagellar motor. This rotary nanomachine is powered by the ion motive force, combining membrane potential and transmembrane ion gradients—protons in *Escherichia coli* and *Salmonella enterica*, or sodium ions in *Vibrio* species [14]. While some bacteria such as *Vibrio cholerae* and *Pseudomonas aeruginosa* possess a single polar flagellum, peritrichous bacteria like *E. coli* and *S. enterica* carry multiple flagella per cell (Figure 1a). These bacteria swim by bundling flagella into a cohesive structure for smooth, forward motion (run) and reorient by unbundling them (tumble). The run-tumble pattern underlies chemotaxis—allowing bacteria to respond to gradients of chemicals, temperature, or oxygen—and is essential for their survival strategy [14].

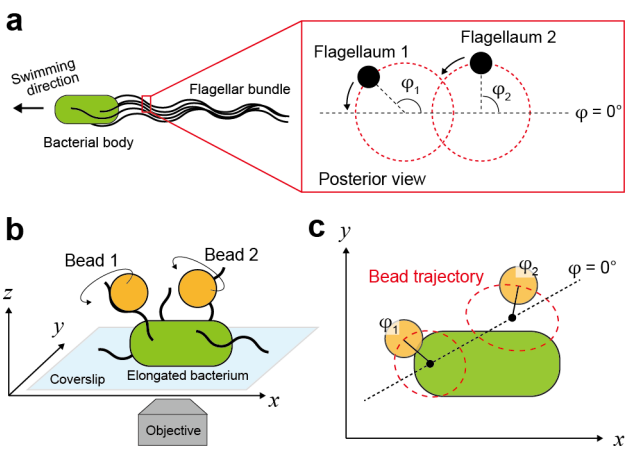

Figure 1. Synchronization in the context of flagellar bundling. (a) Schematic of a peritrichous bacterium swimming with bundled flagella (left). The region indicated by the red box is enlarged (right), showing a posterior view of two flagella and their phase difference. Stable bundle formation requires $\phi_1 \simeq \phi_2$ [15, 16]. (b) Bead assay used to test synchronization of two flagella. (c) Definition of ϕ_1 and ϕ_2 in the bead assay.

Turning to the flagellar bundling mechanism, while similar rotation speeds among flagella are likely essential, might phase alignment between individual left-handed helical filaments also play a role? Addressing this question, macroscale model experiments and simulations have suggested the need for in-phase synchronization to enable bundling [15, 16]. The bending rigidity of bacterial flagella has been reported to lie in the range of 2–4 pN $\cdot$ μm^2, corresponding to a Young's modulus of up to $\sim$ 1 GPa [17, 18].

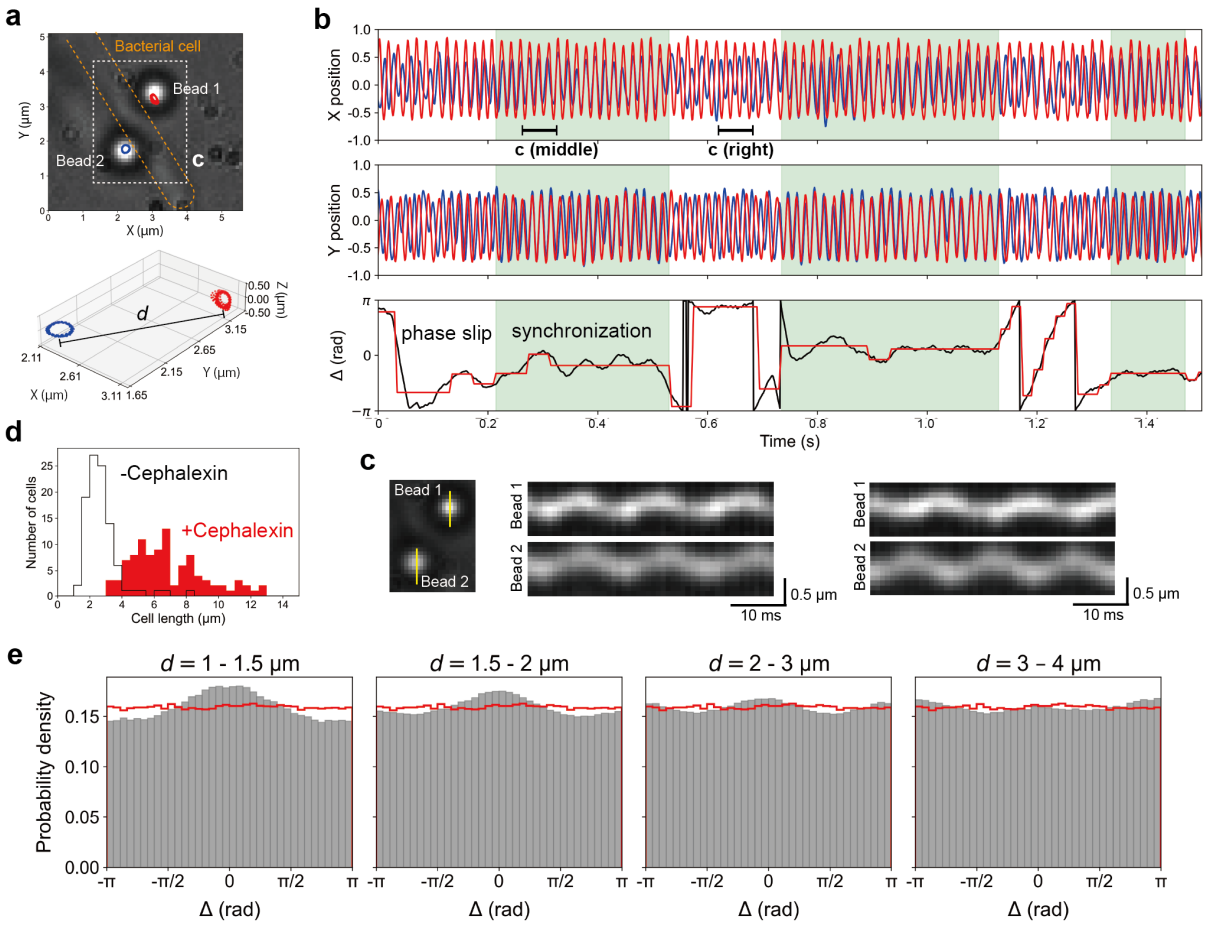

Figure 2. Simultaneous rotation measurements of two neighboring beads. (a) 1-μm beads attached to flagella extending from the same bacterial cell (upper) and 3D rotation trajectories (lower). The addition of cephalexin elongated the bacterial cells. Distances between beads (d) were defined as those between rotational centers. The area indicated by a white box is analyzed in (c). (b) Time variations of bead positions (X and Y) are shown in the upper panel. Data from two beads are discriminated by blue and red. The phase differences (Δ) determined for the time variations of bead positions are shown in the lower panel. The results of stepwise smoothing (see Figure S6) are shown in red. The periods of in-phase synchronization are highlighted in green. See Figures S1 and S2 for additional example data. The kymographs of the periods designated by horizontal bars in the X position are shown in (c). See also Movie 1. (c) Kymographs along the yellow lines in the left panel show in-phase synchronization (middle) and phase slip (right) between Bead 1 and Bead 2. (d) Effect of cephalexin on the cell length. (e) Dependence of the phase-difference distribution on d: 10, 46, 28, and 13 pairs were analyzed for d =1-1.5 μm, 1.5-2 μm, 2-3 μm, and 3-4 μm, respectively. The red lines represent the results for "pseudo pairs" created by randomly pairing beads that were either located sufficiently far apart or observed in different chambers. To assess accidental synchronization, beads with approximately equal intrinsic frequencies were selected for the pseudo pairs.

This modulus is comparable to cytoskeletal proteins in biological systems and to soft plastics or Teflon in engineered materials [19]. Such intrinsic stiffness suggests that constraints on the relative phase between rotating filaments are likely relevant for stable bundle formation. Thus, despite the central importance of flagellar synchronization, direct experimental evidence has remained lacking.

Here, we report transient in-phase rotational synchronization between adjacent bacterial flagella, revealed through optical tracking of microspheres attached to individual filaments. The observed synchronization was sensitive to the inter-bead distance and the rotation-speed difference between flagella. A theoretical model incorporating elastic deformation of flagella and hydrodynamic coupling between rotating beads accounted for the observed behavior. These findings provide direct evidence for hydrodynamically mediated synchronization in peritrichous bacteria and reveal a minimal physical mechanism for bundle initiation.

Results and Discussion

Flagellar synchronous rotation. We carried out a bead assay to measure rotations of two *Salmonella* flagella simultaneously (Figures 1b and 2a). We determined the phases of two beads attached to truncated flagellar filaments (ϕ_1 and ϕ_2) from their rotation trajectories (Figure 1c) and then determined the temporal variation of phase difference between two beads ($\Delta = \phi_1 - \phi_2$). The time courses of bead positions and Δ (Figure 2b) show intermittent in-phase rotations between the two beads, interrupted by occasional phase slips. The kymograph analysis also represents phase coincidence and phase slip between two beads (Figure 2c) .

The addition of cepharexin to the growth media elongated the bacterial body length (Figure 2d), enabling us to investigate if the distance between beads (d) affects their rotations. Analysis of the phase difference distributions obtained from the rotation traces revealed a prominent peak near $\Delta = 0$, indicating in-phase synchronization, and the peak height decreased with an increment of d (Figure 2e). We note here that if the two beads rotate at similar speeds, such in-phase synchronization could arise by chance, even in the absence of any interaction. To control for this possibility, we generated "pseudo pairs" by ran-

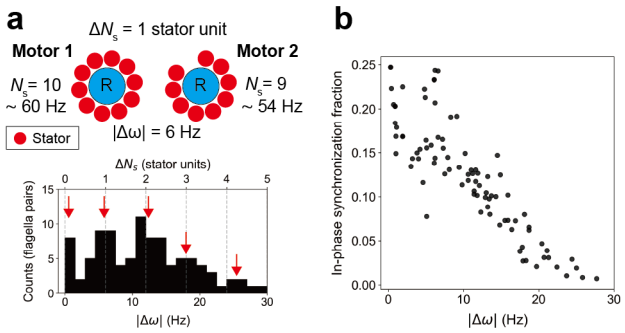

Figure 3. Difference in intrinsic frequencies. (a) Relationship between the number of stators and flagellar motor speed. The flagellar rotor (R) is surrounded by approximately 10 stators. Discrete differences in flagellar rotation rates between motor pairs are associated with differences in the number of stator units (see *main text*). For example, if the speed difference ($|\Delta\omega|$) between Motor 1 and Motor 2 is 6 Hz, the stator-number gap (ΔN_s) is estimated to be 1 unit (upper panel). The lower panel shows the distribution of $|\Delta\omega|$ ($n = 85$ motor pairs). Red arrows indicate approximate peak positions. The ΔN_s values estimated from $|\Delta\omega|$ are indicated on the upper axis, and vertical dashed lines are drawn at 6 Hz intervals. (b) Dependence of the in-phase synchronization fraction on $|\Delta\omega|$. The in-phase synchronous fraction is the ratio of the sum of in-phase synchronous periods, determined from Δ vs time plots as shown in Figure 2b, to total measuring time. Each dot represents a pair of beads.

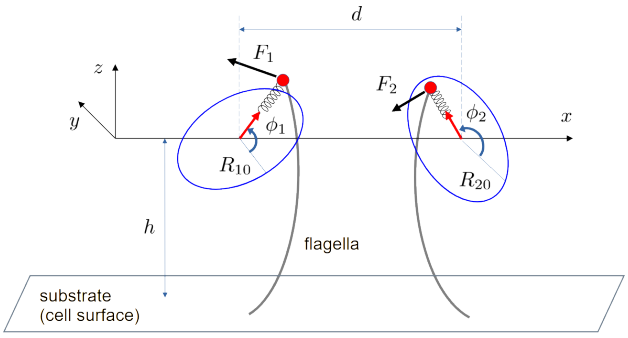

Figure 4. Hydrodynamic model. The beads represent the tethered cells. Their positions are specified by the phases ϕ_1, ϕ_2 and the radial displacements from the circular trajectories of radii R_{10} and R_{20}. See the text and Supplementary Information for details.

domly combining rotation traces of beads that were either spatially well-separated on different cells or obtained from independent experiments conducted in separate observation chambers (see Figure S3 for example rotation data). The peak-distribution analysis of pseudo pairs showed no peak at any specific phase difference for these pseudo pairs (red lines in Figure 2e). These results suggest that neighboring beads experience distance-dependent interactions that intermittently induce in-phase synchronization.

Variation of the intrinsic-frequency difference. We extracted the periods during which the two beads were asynchronized and determined their respective intrinsic frequencies, ω_1 and ω_2 (Figure S4). Focusing on the difference between ω_1 and ω_2 ($= \Delta\omega$), we detected multiple peaks in the distribution that were approximately equally spaced (Figure 3a). The stator units driving the bacterial flagellar motor are known to turn over during rotation [20]. Though ∼10 stator units are incorporated into the flagellar motor, the number of stators can vary between bacterial cells and motors, and may change over time. Such variations of the stator numbers have been observed as a motor-speed distribution with multiple peaks and stepwise changes in motor speed [21, 22]. Rotation assays of the *Salmonella* flagellar motor have shown speed distributions and stepwise speed variation with an interval of 6 - 8 Hz [22], which is consistent with the peak intervals observed in the $\Delta\omega$ (red arrows in Figure 3a). There may have been a difference of up to four stator counts between the motors analyzed as a pair. The $\Delta\omega$ due to this difference in stator number also had a distinct effect on the synchronization of the two beads, showing that the larger the $\Delta\omega$, the smaller the synchronous time fraction (Figure 3b). Although the variation in stator number may have been accentuated by the extension of the cell length with cephalexin, synchronization occurs when the stator number differs by only one or two. The stator number features a mechanosensing-like tuning mechanism for the number of incorporations: It increases with the elevation of external load and decreases with load reduction [23–26]. The number of stators can be adjusted to nearly the same in a load-dependent manner once a bundle is transiently formed, which may then enable stable bundle formation.

Synchronization model introducing elastic deformation. Our nanophotometry experiments revealed that neighboring flagella rotate in phase, often sustained for several tens of revolutions. What mechanism underlies the synchronization of this bacterial nanomachine? To address this question, we focused on hydrodynamic interactions between oscillators—a possibility originally proposed by Taylor in the context of low Reynolds number environments [11]—and conducted a theoretical investigation. In the case of *Chlamydomonas*, breaststroke-like swimming is achieved through a repeated cycle of an effective stroke, where the flagella push fluid forcefully, and a recovery stroke, which slowly returns them to the initial position. A representative class of theoretical models assumes that such periodic modulations of driving torque can lead to hydrodynamic synchronization [27] (see also [28, 29] for reviews). However, although bacterial flagellar torque exhibits stochastic fluctuations, there is no clear evidence for periodic modulation. Another model treats active fluid flow along the flagellar axis as the source of synchronization in bacterial carpets, where the cells are attached to the substrate [30]. However, in the present setup, flow induced by the rotating tethered cell is more important than the flagella-generated axisymmetric flow. This is similar to the situation of elastic cilia, where distortion of the trajectories modulates hydrodynamic interaction and induces synchronization [31]. Building on the previous work, we developed a new theoretical model that emphasizes the role of flagellar elasticity in enabling synchronization.

In our model, each tethered cell is represented by a bead that is driven by a constant force and makes a circular trajectory in the absence of hydrodynamic flow (Figure 4). The flagellar elasticity is mimicked by a harmonic spring that anchors each bead to the center of the circle. The spring is extended by the hydrodynamic forces and adjusts its length on a timescale much shorter than the rotation period. Therefore, the positions of the beads are well described by their phases ϕ_1, ϕ_2 only. The flow field generated by the rotating beads is described by the Stokes law for the drag force and the Blake tensor, the Green

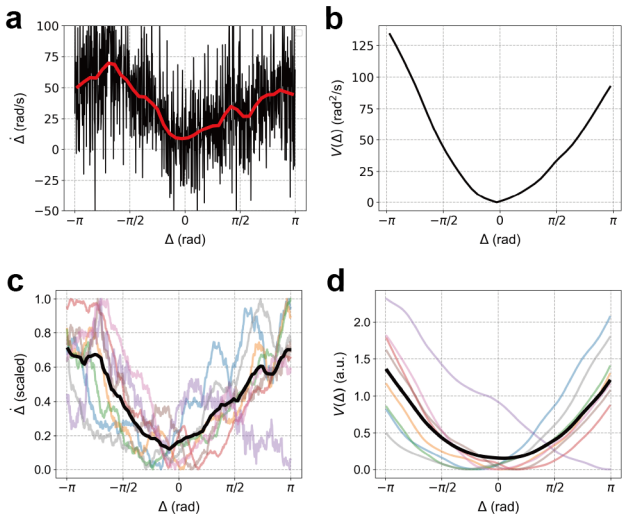

Figure 5. Effective potential inferred from time-varying phase differences. (a) Distribution of $\dot{\Delta}$(see *main text*) against Δ obtained from rotation data of a pair of beads. The red line represents the moving average of the black plots (median of the raw data). (b) An effective potential estimated from (a). (c) $\dot{\Delta}$ vs Δ plots of multiple different pairs of beads scaled by individual minimum values (light colored lines) and their average plot (thick black line). (d) An effective potential estimated from (c) and their average plot (thick black line).

function of the Stokes equation in the presence of a no-slip boundary. In studying synchronization, we focus on the time evolution of the phase difference $\Delta = \phi_1 - \phi_2$. Incorporating small differences in the natural rotation frequencies ω_1, ω_2 and the gyration radii R_{10}, R_{20} of the two beads, we obtain $\dot{\Delta} = d\Delta/dt$ in the form

$$\begin{aligned}\dot{\Delta} = \Delta\omega + \gamma\left(\rho\omega_2 - \rho^{-1}\omega_1\right)\overline{t_{1x}t_{2x}} \\ - \gamma\omega_1\omega_2\tau\left(\rho\overline{e_{1x}t_{2x}} - \rho^{-1}\overline{t_{1x}e_{2x}}\right)\end{aligned} \quad (1)$$

Here, $\gamma = 9ah^2/d^3$ is a geometrical coupling parameter, where a is the bead radius (with $a = 0.5$ μm) and h is the height of the rotational orbit from the surface (~ 1 μm). $\rho = R_{20}/R_{10}$ is the ratio of the intrinsic orbital radii, τ is the radial relaxation time, t_{ix} and e_{ix} are the x-components of the radial and tangential unit vector of the intrinsic orbits, and $\overline{A}$ means as cycle average of any quantity A. For the circular orbits, we obtain

$$\begin{aligned}\dot{\Delta} &= \Delta\omega - C\sin(\Delta - \Delta_0) \\ &= -\frac{dV}{d\Delta},\end{aligned} \quad (2)$$

where C (> 0) and Δ_0 are constants determined the parameters mentioned above, and

$$V(\Delta) = -\Delta\omega \cdot \Delta - C\cos(\Delta - \Delta_0) + \text{const.} \quad (3)$$

is an effective potential [27]; see Supplementary Information for details of the model. Note that Eq.(2) has a stationary (i.e., phase-locking) solution only if $|\Delta\omega| \leq C$.

Phase-locking stability. We assessed the variation rate of Δ, $\dot{\Delta}$, from Δ vs time plots. $\dot{\Delta}$ was calculated approximately every one revolution: $\dot{\Delta}(t) = (\Delta(t+T) - \Delta(t))/T$, where the period T was defined as 20 ms based on an estimated rotation frequency of approximately 50 Hz. The obtained distributions of $\dot{\Delta}$ show convex downward

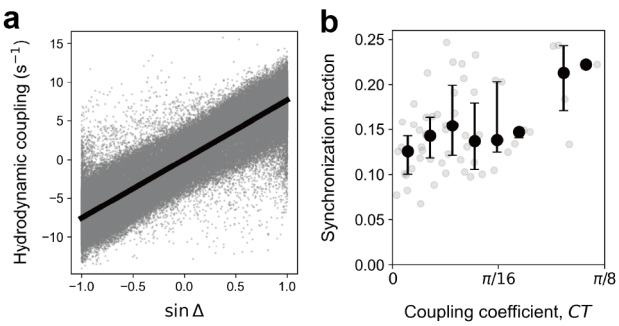

Figure 6. Hydrodynamic coupling. (a) Relationship between hydrodynamic coupling strength and phase difference. The gray dots are values obtained from a time-series data of a pair of beads, and the black line is the result of line fitting. (b) Dependence of in-phase synchronization on the coupling coefficient. The dimensionless coupling coefficient CT is plotted (see *main text* for details). The gray dots indicate data from individual bead pairs. The black dots and error bars represent the median and interquartile range within each bin, where the range 0 to $\pi/8$ was divided into ten equal bins.

with a minimum around $\Delta = 0$ (Figure 5a and c). $\dot{\Delta}$ can be described using the effective potential $V(\Delta)$ as $\dot{\Delta} = -\mathrm{d}V/\mathrm{d}\Delta$, allowing us to estimate the potential landscape for the flagellar synchronization experimentally. As predicted from the $\dot{\Delta}$ distribution, $V(\Delta)$ shows the potential minimum at $\Delta = \Delta_0 \sim 0$ (Figure 5b and d), suggesting the stability of the in-phase synchronous state.

According to calculations that account for the elasticity of the bacterial flagellar filament (~ 3.5 pN $\cdot$ μm^2) [32] and the hook ($\sim 1.6 \times 10^{-4}$ pN $\cdot$ μm^2) [33], together with their lengths and the surrounding viscosity, the time constant τ of flagellar synchronization is estimated to be on the order of 15 ms (Supplementary Information). Experimentally, the time constant for the transition from the asynchronous to the synchronous state was found to be approximately 40 ms (Figure S6), which is of the same order as the theoretical estimate. Although the filament-specific, elasticity-dependent fluctuations in the rotational trajectory that the model predicts to precede synchronization were not clearly resolved, intermittent disturbances of the rotational path were frequently observed during rotation (Figure 2a and b). Measurements with higher spatiotemporal resolution are expected to clarify the relationship between these trajectory disturbances and synchronization.

Synchronization by hydrodynamic coupling. In our model, the hydrodynamic force acts only along the direction connecting the centers of the two orbits (the X-axis in Figure 4), and its magnitude is described by the third term in the time-evolution equation of Δ (hereafter referred to as the interaction term). The position vectors of the beads, the ratio of their orbital radii, and the frequency difference included in this interaction term were experimentally measured in this study. The geometrical factor (γ) and the radial relaxation time of the beads (τ) can be estimated from the bead-assay setup and from literature values (Supplementary Information, see [32, 33] for physical properties of flagella). By averaging this experimentally determined interaction term over one period (assuming Δ remains constant within a cycle), we obtain $C\sin\Delta$ (Eq.(2)). In other words, when the interaction term is plotted against $\sin\Delta$ as in Figure 6a, the slope provides the coefficient C, which represents the interaction

strength (hereafter referred to as the coupling coefficient). Since the interaction term has the dimension of inverse time (s^{-1}), C also has the dimension of s^{-1}. Thus, multiplying C by the oscillation period T (determined from the mean intrinsic frequency of each bead pair) yields the dimensionless coupling coefficient CT. We then examined the relationship between CT and the time fraction of in-phase synchronization observed for each bead pair, and found that larger values of CT correlated with longer synchronization times (Figure 6b).

According to the time-evolution equation of Δ, phase locking (i.e., $\dot{\Delta} \to 0$) requires $|\Delta\omega| \leq C$ as mentioned in the model section. Experimentally, bead pairs with larger $|\Delta\omega|$ were indeed less likely to synchronize (Figure 3b). For example, a typical pair with intrinsic frequencies near 60 Hz and $\Delta\omega = 6\,\mathrm{Hz}$ (roughly one stator difference) would require a coupling strength of $CT > 0.2\pi$ to synchronize, since the phase slip per period is $\Delta\omega \cdot T = 6\,\mathrm{Hz} \cdot (1/60\,\mathrm{s}) \cdot 2\pi = 0.2\pi$. Our analysis included pairs with $|\Delta\omega|$ up to 15 Hz (corresponding to a difference of less than three stators), which would theoretically require $CT > (15/6) \cdot 0.2\pi = \pi/2$ for every pair to be synchronized. Therefore, our estimation $CT < \pi/8$ is consistent with the observed partial synchronization with the time fraction $< 1/4$ (i.e., $\sim$0.25 at its maximum in Figure 6b).

Furthermore, the model assumes that radial relaxation is much faster than the rotation period, requiring $\omega\tau \ll 2\pi$. Given the flagellar elasticity and viscous drag coefficient, we estimate $\tau \sim 15$ ms (Supplementary Information). For $\omega \sim 60$ Hz, this gives $\omega\tau \sim 1$, which satisfies this requirement under our experimental conditions. Taken together, these findings suggest that the hydrodynamic interaction assumed in the theory is indeed the emergent factor underlying synchronization of bacterial flagella.

Theoretically, the coupling constant C scales with the bead distance d and height from the cell surface h as $C \propto h^2/d^3$ (via γ), while its dependence on the orbital radius b is negligible in our approximation (see the Supplementary Information). This assumption is justified by our experimental data, which show a narrower distribution of b than d and small b/d ratios (Figure S7). Considering the relatively constant b and h, we tested the scaling law $CT \propto 1/d^n$. This yielded a best fit with $n = 2.82$ (Figure S7), which is in excellent agreement with the theoretical prediction $n = 3$. This result strongly supports the validity of the long-distance approximation in our model. On the other hand, a large scatter in CT was observed at short distances (Figure S7), which might reflect non-trivial dependencies on the specific orientations of the two orbits [34] that are not captured by our simplified model. Elucidating these effects is a subject for future work and will require experiments with higher spatiotemporal resolution.

Flow around rotating beads. Having established that hydrodynamic interactions can quantitatively account for the observed synchronization, we next sought to directly visualize the underlying flow field. To this end, we introduced tracer beads into the chamber during observations of beads rotating on bacterial flagella and tracked their trajectories. Tracking tracer beads around a single rotating bead revealed a counterclockwise flow pattern consistent with the direction of rotation (Figure 7a). When

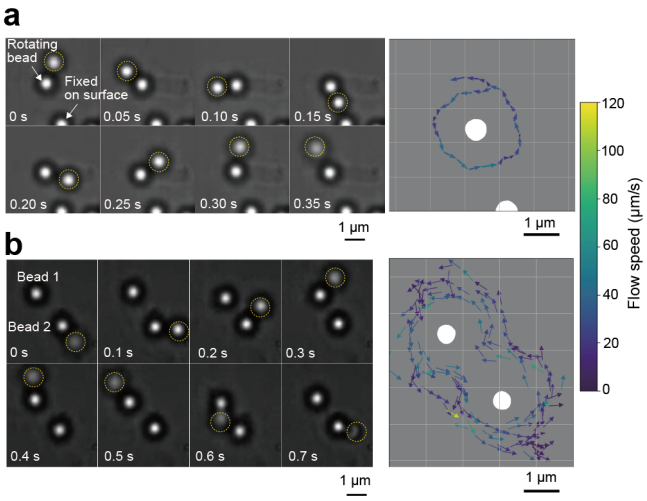

Figure 7. Flow around rotating beads. (a) Movement of a free bead (circled by a yellow dashed line) around a single rotating bead attached to a flagellum (left) and flow estimated from the free-bead movement (right). (b) Movement of a free bead around two rotating beads and the estimated flow. See Movie 2 and Movie 3 for a single bead and paired beads, respectively.

tracer beads were introduced during observations of two beads rotating in close proximity on flagella protruding from the same bacterium, a continuous counterclockwise streamline encompassing both beads was visualized (Figure 7b). These observations suggest that the continuous flow connecting the two beads could contribute to the hydrodynamic coupling underlying their phase-locked rotation.

Conclusion

Our nanophotometry approach revealed that two beads attached to bacterial flagella exhibit intermittent in-phase synchronization when rotating in close proximity. The emergence of synchronization depended on both the distance between the beads and the intrinsic frequency difference of the two flagellar motors, the latter likely arising from variation in the number of stators assembled into each motor. Our hydrodynamic model that incorporates changes in the rotational trajectory due to flagellar filament elasticity showed a correlation between inter-bead fluid interactions and the propensity for synchronization. Tracer-bead experiments visualized a continuous flow surrounding the two rotating beads, suggesting that such a flow may play a role in triggering synchronization. To our knowledge, these findings represent the first demonstration of synchronization in molecular nanomachines operating in living cells.

Bacterial flagella are undoubtedly capable of in-phase synchronization, but does intermittent synchronization confer any advantage to the bacterium? Our study was motivated by the longstanding view, grounded in macroscale observations, that flagellar bundling in peritrichous bacteria requires rotational synchronization. Recent theoretical work has proposed that hydrodynamic interactions along the flows generated by bacterial motion can promote flagellar bundling [35], and directed motion is indeed likely to contribute substantially to this process. In this context, transient episodes of in-phase rotation might play a critical role in nucleating or stabilizing the initial stages of flagellar bundling, while allowing

subsequent adjustments in motor torque or filament orientation. Such a mechanism could enable smooth transitions between swimming and tumbling states, or fine-tune motility according to local environmental conditions. This mechanism may be particularly relevant to microbial pathogenicity, as motility is an essential virulence factor in many flagellated bacteria [36, 37]. Thus, whereas locomotion at high Reynolds numbers relies heavily on neural control, fluid-mediated synchrony at low Reynolds numbers may serve as a fundamental physical mechanism ensuring the robust operation of the bacterial machinery.

Methods

Bacteria and media. *S. enterica* serovar Typhimurium strain MM3076iC [(Δ*cheA–cheZ*), *fliC* (Δ204–292)] was used, which possesses flagellar motors that exclusively rotate counterclockwise with sticky flagellar filaments to be labeled with latex beads [38]. L-broth (LB) and motility medium were prepared as described previously [39]

Bead assay. Bacteria grown overnight in LB at 37°C were diluted 1:100 into fresh LB and incubated for 3h at 37°C with shaking. After adding 20 μg/mL cefalexin to elongate the cell length [40], the mixture was further incubated for 1h at 37°C with shaking. Bacteria collected by centrifugation were suspended into a motility medium and their sticky flagellar filaments were truncated by passing through a 27-gauge needle. The bacterial suspension was infused into a glass chamber to adhere the bacteria to a glass surface, and 1-μm latex beads were infused into the chamber. Unbound beads floating in the chamber were removed by infusing motility medium, and bead rotation was observed under a bright-field microscope (BX53, 100 $\times$ oil immersion objective, Olympus). Rotations of two beads attached to two filaments of the same cells were recorded by a high-speed CMOS camera (IDP-Express R2000, Photron) at intervals of 1 ms and their angular positions were determined using the line connecting the two rotation centers as the origin. See Supplementary Information for details of data analysis.

Data Availability

The data supporting the findings of this study are available from the corresponding author upon request.

Code Availability

The computer codes used for this study are available from the corresponding author upon reasonable request.

References

[1] Marder, E. & Bucher, D. Central pattern generators and the control of rhythmic movements. *Curr. Biol.* **11**, R986–R996 (2001).

[2] Sumpter, D. J. The principles of collective animal behaviour. *Phil. Trans. R. Soc. B* **361**, 5–22 (2006).

[3] Portugal, S. J. *et al.* Upwash exploitation and downwash avoidance by flap phasing in ibis formation flight. *Nature* **505**, 399–402 (2014).

[4] Ashraf, I., Godoy-Diana, R., Halloy, J., Collignon, B. & Thiria, B. Synchronization and collective swimming patterns in fish (hemigrammus bleheri). *J. R. Soc. Interface* **13**, 20160734 (2016).

[5] Li, L. *et al.* Vortex phase matching as a strategy for schooling in robots and in fish. *Nat. Commun.* **11**, 5408 (2020).

[6] Thandiackal, R. & Lauder, G. In-line swimming dynamics revealed by fish interacting with a robotic mechanism. *eLife* **12**, e81392 (2023).

[7] Ito, S. & Uchida, N. Vortex phase matching of a self-propelled model of fish with autonomous fin motion. *Phys. Fluids* **35** (2023).

[8] Machemer, H. Ciliary activity and the origin of metachrony in paramecium: effects of increased viscosity. *J. Exp. Biol.* **57**, 239–259 (1972).

[9] Polin, M., Tuval, I., Drescher, K., Gollub, J. P. & Goldstein, R. E. Chlamydomonas swims with two "gears" in a eukaryotic version of run-and-tumble locomotion. *Science* **325**, 487–490 (2009).

[10] Goldstein, R. E., Polin, M. & Tuval, I. Noise and synchronization in pairs of beating eukaryotic flagella. *Phys. Rev. Lett.* **103**, 168103 (2009).

[11] Taylor, G. I. Analysis of the swimming of microscopic organisms. *Proc. R. Soc. Lond. A* **209**, 447–461 (1951).

[12] Narematsu, N., Quek, R., Chiam, K.-H. & Iwadate, Y. Ciliary metachronal wave propagation on the compliant surface of paramecium cells. *Cytoskeleton* **72**, 633–646 (2015).

[13] Geyer, V. F., Jülicher, F., Howard, J. & Friedrich, B. M. Cell-body rocking is a dominant mechanism for flagellar synchronization in a swimming alga. *Proc. Natl. Acad. Sci. U.S.A.* **110**, 18058–18063 (2013).

[14] Nakamura, S. & Minamino, T. Structure and dynamics of the bacterial flagellar motor complex. *Biomolecules* **14**, 1488 (2024).

[15] Macnab, R. M. Bacterial flagella rotating in bundles: a study in helical geometry. *Proc. Natl. Acad. Sci. U.S.A.* **74**, 221–225 (1977).

[16] Kim, M., Bird, J. C., Van Parys, A. J., Breuer, K. S. & Powers, T. R. A macroscopic scale model of bacterial flagellar bundling. *Proc. Natl. Acad. Sci. U.S.A.* **100**, 15481–15485 (2003).

[17] Fujime, S., Maruyama, M. & Asakura, S. Flexural rigidity of bacterial flagella studied by quasielastic scattering of laser light. *J. Mol. Biol.* **68**, 347–359 (1972).

[18] Shen, X., Tran, P. N., Tay, B. Z. *et al.* Bending stiffness characterization of bacillus subtilis' flagellar filament. *Biophys. J.* **121**, 1975–1985 (2022).

[19] Howard, J. *Mechanics of Motor Proteins and the Cytoskeleton* (Sinauer Associates, Sunderland, MA, 2001).

[20] Leake, M. C. *et al.* Stoichiometry and turnover in single, functioning membrane protein complexes. *Nature* **443**, 355–358 (2006).

[21] Reid, S. W. *et al.* The maximum number of torque-generating units in the flagellar motor of escherichia coli is at least 11. *Proc. Natl. Acad. Sci. U.S.A.* **103**, 8066–8071 (2006).

[22] Suzuki, Y. *et al.* Effect of the mota (m206i) mutation on torque generation and stator assembly in the salmonella h+-driven flagellar motor. *J. Bacteriol.* **201**, 10–1128 (2019).

[23] Tipping, M. J., Delalez, N. J., Lim, R., Berry, R. M. & Armitage, J. P. Load-dependent assembly of the bacterial flagellar motor. *mBio* **4**, 10–1128 (2013).

[24] Nord, A. L., Sowa, Y., Steel, B. C., Lo, C.-J. & Berry, R. M. Speed of the bacterial flagellar motor near zero load depends on the number of stator units. *Proc. Natl. Acad. Sci. U.S.A.* **114**, 11603–11608 (2017).

[25] Nord, A. L. *et al.* Catch bond drives stator mechanosensitivity in the bacterial flagellar motor. *Proc. Natl. Acad. Sci. U.S.A.* **114**, 12952–12957 (2017).

[26] Lele, P. P., Hosu, B. G. & Berg, H. C. Dynamics of mechanosensing in the bacterial flagellar motor. *Proc. Natl. Acad. Sci. U.S.A.* **110**, 11839–11844 (2013).

[27] Uchida, N. & Golestanian, R. Generic conditions for hydrodynamic synchronization. *Phys. Rev. Lett.* **106**, 058104 (2011).

[28] Golestanian, R., Yeomans, J. M. & Uchida, N. Hydrodynamic synchronization at low reynolds number. *Soft Matter* **7**, 3074–3082 (2011).

[29] Uchida, N., Golestanian, R. & Bennett, R. R. Synchronization and collective dynamics of flagella and cilia as hydrodynamically coupled oscillators. *J. Phys. Soc. Jpn.* **86**, 101007 (2017).

[30] Uchida, N. & Golestanian, R. Synchronization and collective dynamics in a carpet of microfluidic rotors. *Phys. Rev. Lett.* **104**, 178103 (2010).

[31] Niedermayer, T., Eckhardt, B. & Lenz, P. Synchronization, phase locking, and metachronal wave formation in ciliary chains. *Chaos* **18** (2008).

[32] Darnton, N. C. & Berg, H. C. Force-extension measurements on bacterial flagella: triggering polymorphic transformations. *Biophys. J.* **92**, 2230–2236 (2007).

[33] Sen, A., Nandy, R. K. & Ghosh, A. N. Elasticity of flagellar hooks. *Microscopy* **53**, 305–309 (2004).

[34] Uchida, N. & Golestanian, R. Hydrodynamic synchronization between objects with cyclic rigid trajectories. *Eur. Phys. J. E* **35**, 135 (2012).

[35] Chamolly, A. & Lauga, E. Direct versus indirect hydrodynamic interactions during bundle formation of bacterial flagella. *Phys. Rev. Fluids* **5**, 123102 (2020).

[36] Haiko, J. & Westerlund-Wikström, B. The role of the bacterial flagellum in adhesion and virulence. *Biology* **2**, 1242–1267 (2013).

[37] Stevens, J. M., Galyov, E. E. & Stevens, M. P. Actin-dependent movement of bacterial pathogens. *Nat. Rev. Microbiol.* **4**, 91–101 (2006).

[38] Nakamura, S. *et al.* Effect of intracellular ph on the torque–speed relationship of bacterial proton-driven flagellar motor. *J. Mol. Biol.* **386**, 332–338 (2009).

[39] Minamino, T., Imae, Y., Oosawa, F., Kobayashi, Y. & Oosawa, K. Effect of intracellular ph on rotational speed of bacterial flagellar motors. *J. Bacteriol.* **185**, 1190–1194 (2003).

[40] Nishiguchi, D., Nagai, K. H., Chaté, H. & Sano, M. Long-range nematic order and anomalous fluctuations in suspensions of swimming filamentous bacteria. *Phys. Rev. E* **95**, 020601 (2017).

Acknowledgements

We thank Dr. S. Toyabe (Tohoku University) for providing software for rotation analysis. This work was supported by the JSPS KAKENHI: 21H05306 and 22H04828 for SN, and 24K0985 for NU.

Author contribution

SN and NU designed the project. TI and SN set up the optical system and performed the experiments. NU performed theoretical research. All authors wrote the manuscript and approved the submitted version.

Competing interests

The authors declare no competing interests.